ACS NANO

www.acsnano.org

ARTICLE

Single Molecule Protein Detection with Attomolar Sensitivity Using Droplet Digital Enzyme-Linked Immunosorbent Assay

Limor Cohen,[⊥] Naiwen Cui,[⊥] Yamei Cai, Padric M. Garden, Xiang Li, David A. Weitz, and David R. Walt*

Cite This: https://dx.doi.org/10.1021/acsnano.0c02378

Read Online

ACCESS | Metrics & More | Article Recommendations | Supporting Information

ABSTRACT: Many proteins are present at low concentrations in biological samples, and therefore, techniques for ultrasensitive protein detection are necessary. To overcome challenges with sensitivity, the digital enzyme-linked immunosorbent assay (ELISA) was developed, which is 1000× more sensitive than conventional ELISA and allows sub-femtomolar protein detection. However, this sensitivity is still not sufficient to measure many proteins in various biological samples, thereby limiting our ability to detect and discover biomarkers. To overcome this limitation, we developed droplet digital ELISA (ddELISA), a simple approach for detecting low protein levels using digital ELISA and droplet microfluidics. ddELISA achieves maximal sensitivity by improving the sampling efficiency and counting more target molecules. ddELISA can detect proteins in the low attomolar range and is up to 25-fold more sensitive than digital ELISA using Single Molecule Arrays (Simoa), the current gold standard tool for ultrasensitive protein detection. Using ddELISA, we measured the LINE1/ORF1 protein, a potential cancer biomarker that has not been previously measured in serum. Additionally, due to the simplicity of our device design, ddELISA is promising for point-of-care applications. Thus, ddELISA will facilitate the discovery of biomarkers that have never been measured before for various clinical applications.

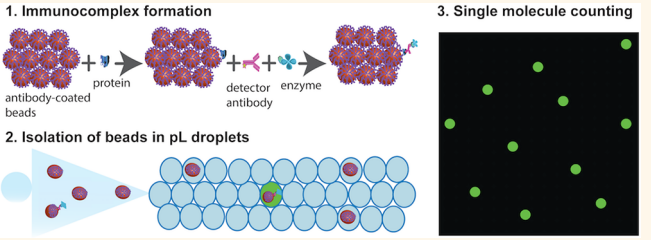

KEYWORDS: *single molecule, ultrasensitive detection, immunoassay, biomarkers, clinical diagnostics, droplet microfluidics*

Proteins are important biomarkers for disease detection, monitoring, and treatment.[1−3] Many proteins are present at low levels in biological samples, and therefore, techniques for ultrasensitive protein detection are necessary.[4] To overcome limitations in sensitivity, the digital enzyme-linked immunosorbent assay (ELISA) was developed, which is 1000× more sensitive than conventional ELISA.[5−10] Digital ELISA enabled detection and discovery of biomarkers in the sub-femtomolar range.[11] However, for many clinical applications, this sensitivity is still not sufficient. Some proteins, such as neurological proteins that are present at low levels in the blood due to difficulty crossing the blood-brain barrier[12] and cancer biomarkers,[13] are still unmeasurable due to inadequate sensitivity. Furthermore, it is challenging to detect many proteins in various other biological samples, such as urine and saliva, due to limitations in sensitivity. Ultrasensitive methods will also improve our ability to measure other biomarkers, such as nucleic acids, which are present at low levels in many biological samples.[14] Thus, improving the sensitivity of current detection methods will facilitate biomarker discovery for clinical applications.

A major barrier to detecting low protein concentrations and improving the sensitivity is low sampling of rare events. While digital immunoassays have improved the sensitivity of conventional analog-based immunoassays by counting single target molecules, limited ability to sample and count a sufficient number of target molecules leads to a compromise in sensitivity. To illustrate this concept, a 10 aM sample has ∼600 molecules in 100 μL. Assuming perfect sampling efficiency, the digital measurement would result in 600 positive events. However, if the sampling efficiency is only 10%, the digital measurement would result in 60 positive events. The Poisson error is the square root of the number of measurements obtained, therefore making more measurements results in less uncertainty. Thus, improving the sampling efficiency

Received: March 19, 2020
Accepted: June 26, 2020
Published: June 26, 2020

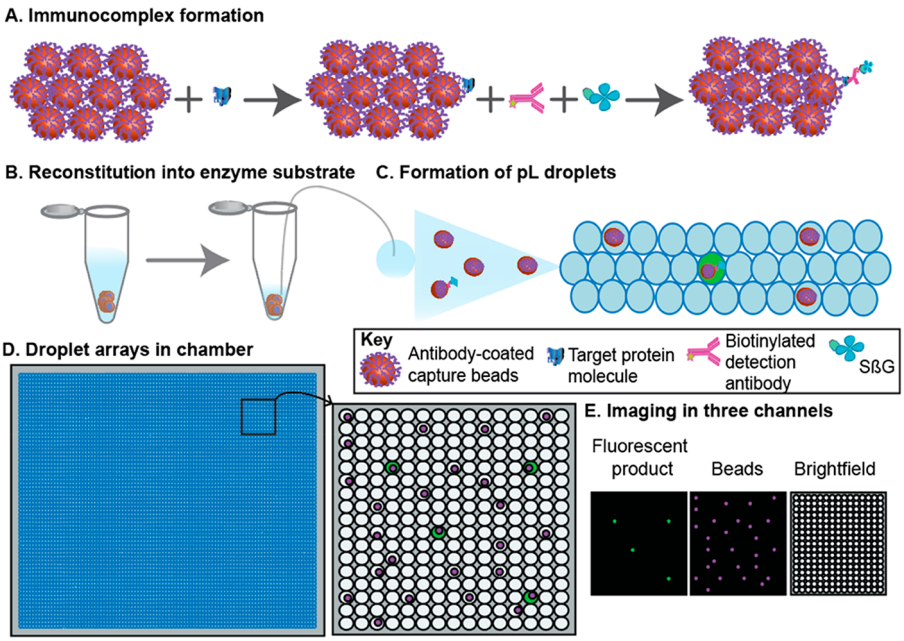

Figure 1. Single molecule protein detection using ddELISA. (A) Bead-based sandwich immunoassay. Here, 100,000 antibody-coated paramagnetic beads are added to a sample containing target protein molecules. A biotinylated detection antibody and Sβ G are then added and bind to the target protein molecule, forming an enzyme-labeled immunocomplex. Based on Poisson statistics, most of the beads will have zero immunocomplexes and a small fraction will have one immunocomplex. (B) The beads are then reconstituted in 2 μL of enzyme substrate. (C) The 2 μL mixture containing the beads and substrate is then partitioned into picoliter droplets. (D) The droplets are loaded into a chamber, forming droplet arrays. (E) Images are obtained in three channels to identify the "on" droplets, the beads, and the droplets.

and counting more molecules should lead to enhanced sensitivity.

It is difficult to improve the sampling efficiency and to increase the number of molecules that are counted. In digital ELISA using Single Molecule Arrays (Simoa), the current gold standard method for ultrasensitive detection, excess antibody-coated beads compared to the number of target molecules are used, such that most beads will not bind any target molecules while a small percentage of beads will bind a single target molecule. In this way, a single protein molecule is captured on a bead. The protein is then labeled with an enzyme and the beads are isolated into femtoliter sized wells such that each well can only fit one bead. After the array is sealed with oil, wells containing an enzyme-labeled immunocomplex generate a locally high concentration of fluorescent product, enabling single molecule detection by counting active wells. To ensure maximal sensitivity, it is necessary to analyze many beads, and in turn, positive events. However, it is challenging to isolate beads and an external force is often used to facilitate bead loading into the wells.[15] In the Simoa HD-1 Analyzer, beads are isolated inside wells via gravity.[16] Yet, only ∼5% of the total assay beads used are isolated and analyzed, leading to a compromise in sensitivity.[16] Improving the loading efficiency of paramagnetic beads can be accomplished by applying a magnetic force. Others have used an electric field and showed improvements in bead loading;[17] however, the implications on immunocomplex formation and improvement of assay sensitivity have largely not been investigated. Despite these bead loading approaches, development of simple approaches that can improve bead loading efficiency, and in turn also lead to enhanced sensitivity, remains limited.

One simple approach to improve sampling of rare events is by entrapping beads in water-in-oil droplets.[18] Droplets are advantageous for this application for several reasons. The first is the ability to entrap a high percentage of the beads for analysis with minimal bead loss, which can lead to high sensitivity. The second is the simplicity of droplet generating devices and the lack of a need for costly and complicated ultrafine structures. The third is the ability to use a simple optical setup for droplet imaging. Furthermore, droplet generation is a very fast process, with an ability to easily generate millions of droplets in a few minutes. These features make droplet microfluidics advantageous for development of highly sensitive digital assays. Droplet microfluidics assays have been previously developed for various applications, including droplet digital PCR,[19,20] nucleic acid sequencing,[21,22] and single cell analysis.[23,24] Droplet microfluidics assays have also been developed for proteins, particularly for detecting secreted molecules from single cells.[25−27] Others have also used droplet microfluidics to develop digital protein immunoassays, however, have not demonstrated improved sensitivity over the state-of-the art techniques for ultrasensitive protein detection.[28,29]

Here, we developed an approach for ultrasensitive, single-molecule detection of proteins using digital ELISA and droplet microfluidics. This approach, which we refer to as droplet digital ELISA (ddELISA), allows us to sample low numbers of molecules, thereby reducing measurement uncertainty and increasing sensitivity. Our approach demonstrates high sensitivity in the low attomolar range, with improvements of up to approximately 25-fold in sensitivity over Simoa, which is the current gold-standard method for ultrasensitive protein detection. Using ddELISA, we measured the LINE1/ORF1 protein, a potential cancer biomarker that has not been previously measured in serum. Additionally, due to the simplicity of our device design, ddELISA is promising for point-of-care (POC) applications.

https://dx.doi.org/10.1021/acsnano.0c02378
ACS Nano XXXX, XXX, XXX−XXX

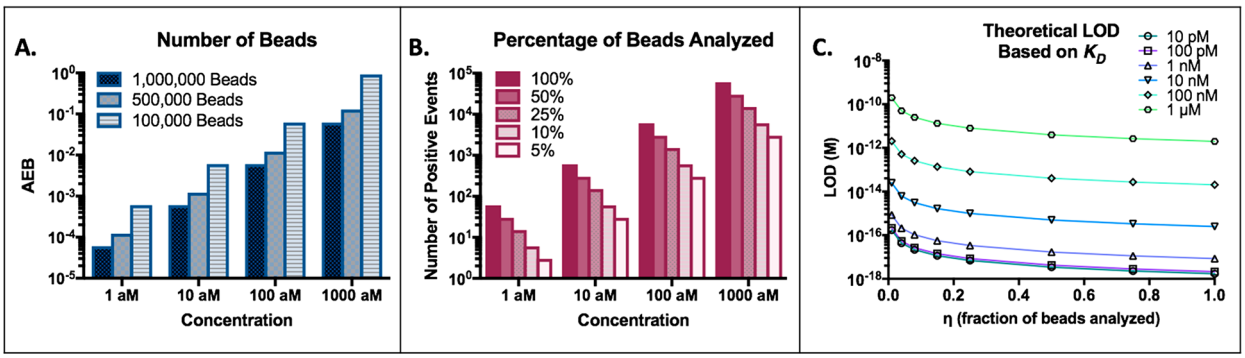

Figure 2. Theoretical calculations. (A) AEB at various concentrations using different numbers of beads. For a given concentration, as the number of beads increases, the AEB decreases. (B) Digital measurement (number of positive events) at various concentrations when different percentages of beads are analyzed. As the percentage of beads analyzed increases, so does the number of positive events. (C) Theoretical LOD at different K_D's.

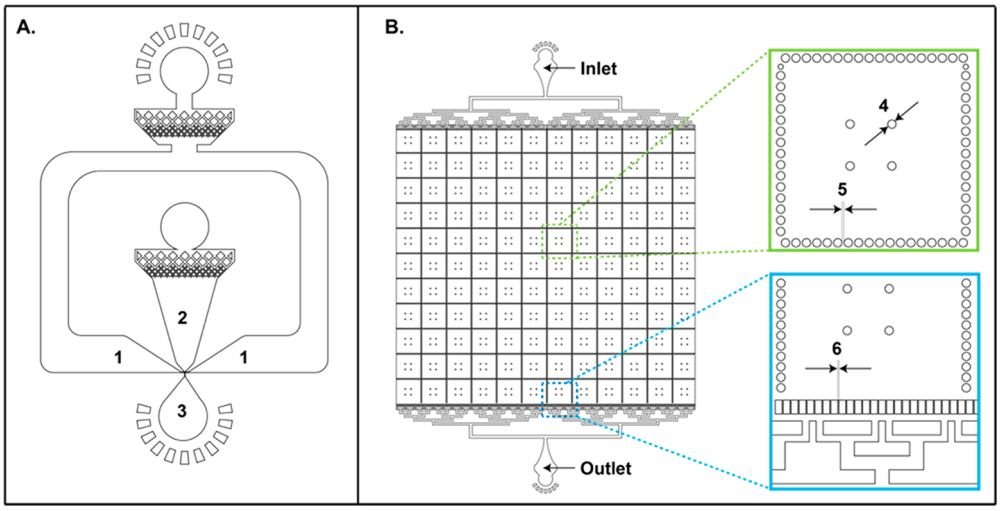

Figure 3. ddELISA device design. (A) The droplet generating device has two inlets, one for the oil with surfactant (1) and one for the beads with substrate mixture (2). The outlet (3) is used to collect the droplets. The width of the channel at the junction is 9 μm, and the smallest feature is 5 μm at the junction. The overall dimensions of the device are 4.5 mm × 7 mm. (B) The chamber for the droplet arrays contains an inlet and an outlet. The blue panel shows the blocking posts, which are used to prevent droplets (diameter of 14 μm) from escaping. The distance between two posts (6) is 7 μm. The green panel shows one of 132 subchambers. The post diameter (4) is 60 μm, and the spacing between two posts is 20 μm (5). The dimensions of the entire chamber are 16 mm × 24 mm.

RESULTS AND DISCUSSION

Single Molecule Detection of Proteins using ddELISA.

ddELISA is a bead-based digital immunoassay in which beads are isolated in picoliter-sized droplets and then loaded into a chamber, forming droplet arrays, for analysis (Figure 1). More specifically, antibody coated paramagnetic beads are added to a sample containing the target molecule (Figure 1A). The target molecule is then labeled with a biotinylated detection antibody and streptavidin-β-galactosidase (SβG), forming an enzyme-labeled immunocomplex. The beads are then resuspended in a small volume (2 μL) of substrate, fluorescein di-β-D-galactopyranoside (FDG) (Figure 1B), and the mixture is partitioned into picoliter droplets such that most droplets have zero beads and a small percentage has one bead (Figure 1C). The droplets are then loaded into a chamber in a monolayer to form droplet arrays (Figure 1D). Images in three channels are obtained to identify (i) the droplets, (ii) the beads, and (iii) the fluorescent product and thus the "on droplets" (Figure 1E). The signal output is measured using the unit of average enzymes per bead (AEB).[30]

The assay setup is similar to that of the conventional automated Simoa platform with three major differences. The first is a reduction in the number of beads used. A conventional Simoa uses 500,000 beads, while in ddELISA we use 100,000 beads. Reducing the number of beads can increase the signal, since the "fraction on" (f_{on}) is the ratio of "on events" to the total number of beads. A lower number of beads will result in a higher f_{on}, thereby leading to a higher signal. Additionally, reducing the number of beads simplifies the assay and makes ddELISA more amenable to POC. Reducing the number of beads using a conventional microwell array is challenging and leads to lower numbers of beads being available for analysis.[31] The second is the digital readout system in which the beads are trapped in picoliter droplets instead of femtoliter-sized wells. The third is the use of FDG as the substrate instead of resorufin β-D-galactopyranoside (RGP), which is used in the conventional Simoa. We selected FDG due to its relatively high stability in droplets.[32] Other than these differences, the assay format is similar to the conventional Simoa. By implementing these changes, we sought to both improve the sensitivity of the conventional Simoa and make it amenable to a POC format.

https://dx.doi.org/10.1021/acsnano.0c02378
ACS Nano XXXX, XXX, XXX−XXX

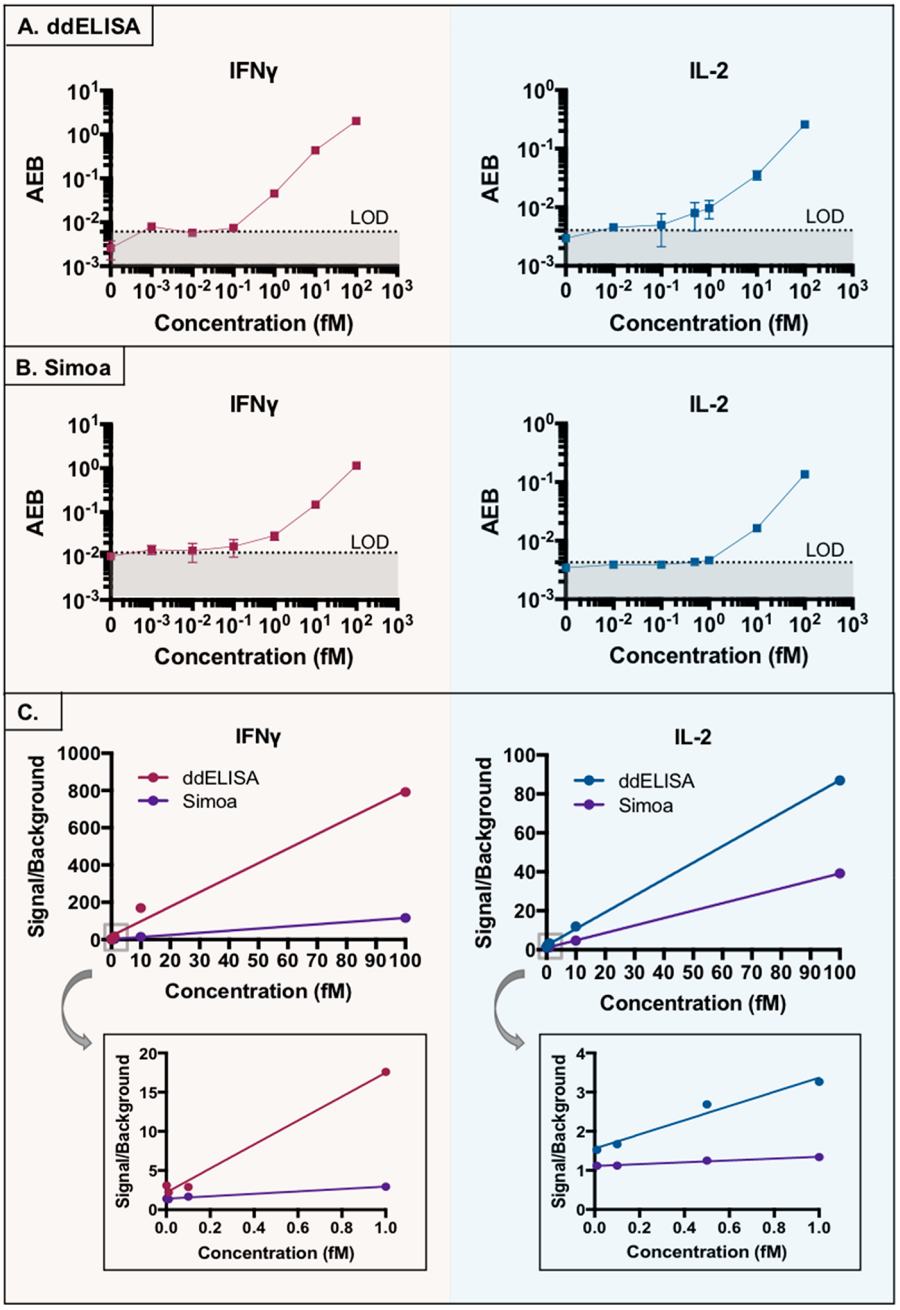

Figure 4. Calibration curves. (A) Calibration curves for ddELISA for IFNγ and IL-2. (B) Simoa assays using the HD-1Analyzer for IFNγ and IL-2. (C) Signal over background for the calibration curve (top). Zoomed in view from 0.0001 to 1 fM for IFNγ and 0.001 to 1fM for IL-2 for both the ddELISA and Simoa assays (bottom).

Theoretical Calculations for Improving Sensitivity. Two important parameters for digital ELISA assays to achieve maximal sensitivity are the number of beads used and the percentage of beads analyzed. The first parameter, the number of beads used, is important since it will determine the f_{on} (the number of positive events over the total number of beads) and the AEB (average enzymes per bead). In 100 μL of a 10 aM sample, there are ~600 molecules. Thus, when 1,000,000, 500,000, and 100,000 beads are used, the theoretical AEB is 0.0006, 0.0012, and 0.0060, respectively. As a result, using fewer beads will lead to a higher f_{on} and AEB (Figure 2A). The second parameter, the percentage of beads analyzed, is important, since at low numbers of molecules it is essential to measure as many positive events as possible to reduce the measurement uncertainty (Figure 2B). For example, in a sample with 600 molecules, if 100% of the beads are analyzed, the digital measurement is 600 positive events, assuming 100% capture and labeling efficiency. If 10% of the beads are analyzed, the digital measurement is 60 positive events. Thus, increasing the percentage of beads analyzed should enable more sensitive detection since the uncertainty in the measurement is reduced. We note that the first parameter, the number of beads used, does not matter if all the beads are analyzed. While analyzing all the beads may be advantageous, it may also result in more complex systems and instrumentation that are not amenable for routine or rapid use. Therefore, by reducing the number of beads used, we can achieve improved sensitivity since the measured signal will be higher.

https://dx.doi.org/10.1021/acsnano.0c02378
ACS Nano XXXX, XXX, XXX−XXX

While better sampling of rare events can lead to improved sensitivity, the sensitivity of digital ELISA is also limited by the dissociation constants of the antibodies. It is possible to achieve zeptomolar sensitivity even with low sampling of 10% of the beads when the dissociation constants are low, such as when using biotin−streptavidin instead of antibodies.[9] Therefore, we sought to understand how the percentage of beads that are analyzed affects the sensitivity of digital ELISA when accounting for the antibody dissociation constants. Figure 2C shows the Poisson noise limited limit of detection (LOD) and bead loading efficiency η at different K_D values. A higher η leads to improvement in sensitivity. The sensitivity of the assay can be improved by about an order of magnitude, regardless of the K_D value, when η increases from 5% to 50%. Furthermore, as expected, lower K_D values result in higher sensitivity. The derivations are provided in the Supporting Information.

Device Design. To improve the sensitivity of ddELISA, we designed a microfluidic device for efficiently generating droplets and packing them into a chamber for analysis (Figure 3). After formation of the immunocomplex on the beads, the beads are suspended in a small, 2 μL volume, of substrate and then partitioned into picoliter-sized droplets. For single molecule analysis, one bead should be isolated in a droplet. Thus, based on the Poisson distribution, most droplets contain no beads and a small percentage of droplets contain one bead. To isolate one bead per droplet, the number of droplets we generate is ∼1,000,000 and the number of beads we use is 100,000.

To simplify the device for POC applications and reduce imaging times, we sought to generate a minimal number of droplets, while still ensuring that each droplet contains either zero beads or one bead for digital analysis. Therefore, our droplet generating device contains two inlets, one for the oil with surfactant and one for the beads and substrate mixture. Many other droplet-based assays contain multiple inlets for assay reagents, resulting in larger input volumes that lead to a larger number of droplets that must be analyzed. In our device, we premixed the fluorogenic substrate with the beads and then added the mixture to the inlet to generate droplets. Using this approach, droplets are formed at ∼20,000 droplets/s, for a total of ∼1 min. Due to the larger volume of the droplets (pL) compared to the volume of the traditional Simoa microwells (fL), the background signal from the enzymatic reaction occurring due to premixing with substrate is low. Following droplet generation, the droplets are then loaded into a chamber for imaging.

To maximize the percentage of beads analyzed, the microfluidic device was designed for optimal performance and minimal sample loss both during droplet formation and during droplet loading into the chamber. In the first step, it is difficult to ensure droplet stability from start of droplet generation due to the low input volume (2 μL) while still generating many droplets per second. To generate many droplets per second, a pump-driven droplet generation system is preferred to a vacuum driven system. However, pump-driven systems often suffer from low droplet stability during the initial droplet generation. To solve this issue, we added oil before loading the aqueous bead solution into the tubing (Supplementary Figure S5) such that the oil is injected first into the channel, which stabilizes the system.

The second step, the design of the imaging chamber and the process of loading the droplets into the chamber, was also optimized. To minimize droplet loss and maximize droplet packing within the imaging chamber, we loaded the droplets and oil into the syringe tubing with the tip of the tubing pointing downward so that the droplets flow to the top due to gravity and the low density of the aqueous phase compared to the oil phase. Once droplet packing is achieved, the droplets are injected into the imaging chamber. To achieve good image quality, droplets must be stationary during imaging. Thus, we designed posts with a spacing of 20 μm for each viewing area so that the droplets, which have a diameter of 14 μm, can squeeze through the posts during loading and then remain fixed in position after loading. A droplet blocking feature with 7 μm posts was added near the outlet to prevent the droplets from escaping the device. Additionally, the imaging chamber was designed such that the droplets were packed in a monolayer, and thus, the height of the chamber (10 μm) was comparable to the diameter of the droplets (14 μm). Due to the shallow height (10 μm) of the microfluidic device, posts with 60 μm diameter are used throughout the device to prevent the chamber from collapsing. Using a combination of these features, we were able to efficiently load the droplets into the chamber in a monolayer for imaging. Using this approach, we can analyze up to 60% of the beads, facilitating ultrasensitive detection.

ddELISA for Ultrasensitive Protein Detection. We evaluated the performance of ddELISA by measuring two protein targets, IFNγ and IL-2, which are present at low levels in many biological samples. The calibration curves are shown in Figure 4A. At low protein concentrations, most of the droplets contain no target protein molecule, and as the concentration increases, a small percentage of droplets contains more than one molecule. Representative histograms of the signals in the bead-containing droplets are shown for various concentrations in Supplementary Figure S6. As the concentration increases, a second population can be observed, indicating that some droplets have more than one enzyme at higher concentrations. We also compared our results to the Simoa assay using the HD-1 Analyzer (Quanterix) and the calibration curves are shown in Figure 4B. We then calculated the signal over the background for both ddELISA and the conventional Simoa and observe a greater signal increase for ddELISA (Figure 4C). We also calculated the detection limits (LODs) as three standard deviations above the background and the quantification limits (LOQs) as 10 standard deviations above the background for ddELISA and Simoa (Table 1). Table 1 also shows the LODs for commercially available Simoa assays. We show that we can achieve LODs in the attomolar range using our approach, an ∼25-fold improvement over the

Table 1. Calculated Limits of Detection (LODs) and Limits of Quantification (LOQs) for IFNγ and IL-2 Using ddELISA and the Conventional Simoa[a]

	LODs and LOQs for ddELISA and Simoa				
	ddELISA LOD (3×)	Simoa LOD (3×)	Quanterix LOD (2.5×)	ddELISA LOQ (10×)	Simoa LOQ (10×)
IFNγ	30 aM	350 aM	1.00 fM	260 aM	1.24 fM
IL-2	20 aM	550 aM	730 aM	360 aM	2.17 fM

[a]The LODs for ddELISA and Simoa were calculated as 3 standard deviations above the background. The LOQs for ddELISA and Simoa were calculated as 10 standard deviations above the background. The LODs for commercially available assays from Quanterix were calculated as 2.5 standard deviations above the background.

https://dx.doi.org/10.1021/acsnano.0c02378
ACS Nano XXXX, XXX, XXX−XXX

conventional Simoa. Since the LOD is calculated from three components, namely, the background levels, the standard deviation over the background, and the calibration curve, improvements in the signal over the background (i.e., the calibration curve) can lead to improvements in sensitivity. Compared to the conventional Simoa, the signal over the background is substantially higher in ddELISA, and thus ddELISA has improved sensitivity. Reducing the number of beads by 5-fold and increasing the number of beads analyzed allowed us to obtain this improvement in sensitivity. Finally, to ensure we can reliably detect proteins in serum, we tested three serum samples per marker and compared our results to Simoa. The two methods show good agreement (Figure 5). Thus, using our approach we can reliably measure proteins with high sensitivity over the current gold standard method for ultrasensitive protein measurements.

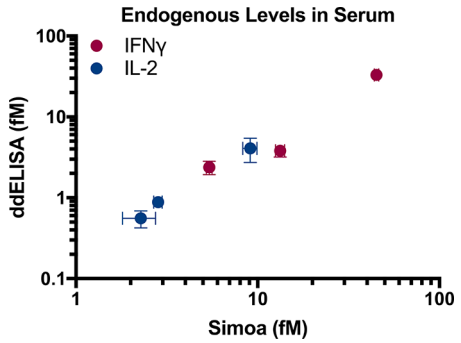

Figure 5. Endogenous protein measurements in serum. IFNγ and IL-2 levels were measured in serum using both ddELISA and the conventional Simoa. Concentrations shown are measured values. The Pearson correlation coefficient is 0.987.

We also developed a ddELISA assay for LINE1/ORF1, a protein that is expressed in many types of cancer tissues.[33−35] To the best of our knowledge, this protein has never been previously measured in serum. In preliminary work (unpublished), we were unable to measure this protein in most samples using conventional Simoa. We used a nanobody as the capture and a biotinylated IgG antibody as the detector. We measured a calibration curve using both ddELISA (Figure 6A) and the conventional Simoa (Figure 6B). The calculated LODs for ddELISA and the conventional Simoa are 290 and 890 aM, respectively. We also calculated the signal over the background for both ddELISA and the conventional Simoa and observe a greater signal increase at low concentrations for ddELISA compared to Simoa (Figure 6C). We note that at higher concentrations, the conventional Simoa performed better than ddELISA. This better performance may be attributed to the higher number of beads used in Simoa.

To determine the minimum percentage of beads necessary to achieve optimal sensitivity, we randomly selected a subset of the beads for analysis and calculated the LODs for each of the IFNγ, IL-2, and ORF-1 ddELISAs. Based on these results, we observe a substantial increase in sensitivity when the percentage of beads analyzed increases from 5% to 20% (Supplementary Figure S7). We also observe that analyzing approximately 20% of the beads using the ddELISA assay format is sufficient to achieve optimal sensitivity. These results are consistent with our theoretical calculations.

To assess the ability of ddELISA to measure endogenous ORF1 in serum, we selected samples from healthy and breast cancer subjects. We measured these samples using both ddELISA and the conventional Simoa (Figure 6D,E). For the healthy subjects, two subjects were detectable using ddELISA while no subjects were detectable using the conventional Simoa. For the cancer subjects, five subjects were detectable using ddELISA and two subjects were detectable using the conventional Simoa. These results suggest that the improved ability of ddELISA to measure serum samples is due the lower LOD of ddELISA.

CONCLUSIONS

We developed an approach for ultrasensitive protein detection based on digital ELISA and droplet microfluidics. A major barrier to improving the detection limit of digital ELISA is low sampling of rare events. Low sampling in digital bead-based immunoassays is typically due to low bead loading efficiencies into femtoliter wells, which results in a compromise in sensitivity since only a small percentage of the "on" beads are analyzed. We designed a simple device that improves our ability to sample low numbers of protein molecules, leading to enhanced sensitivity. In our approach, we reconstitute the bead-based immunocomplexes into a small volume and then isolate single beads into droplets. We then efficiently pack the droplets in an array configuration in a chamber with minimal droplet loss for analysis. Using our approach, we can achieve detection limits in the attomolar range and demonstrate up to ∼25-fold improvement in sensitivity over the conventional Simoa, the current gold-standard for ultrasensitive protein detection. We also note that others have demonstrated that better sampling can improve the ability to detect low abundance molecules.[36,37]

Further improvements in our ability to detect low levels of protein molecules using a digital ELISA assay format is dependent on better binding reagents with low dissociation constants. Ultrasensitive detection of molecules in the zepotomolar range using Simoa was accomplished when biotin−streptavidin, which has a low binding constant, was used.[9] Our lowest calculated LOD is 20 aM, which corresponds to ∼1200 protein molecules. Further improving the sensitivity of digital ELISA and obtaining LODs in the zeptomolar range should be achievable by using better binding reagents.

Another challenge with ultrasensitive protein detection tools is the ability to measure protein biomarkers with high sensitivity at the POC. Ultrasensitive detection of protein biomarkers at the POC has many potential applications,[38] including detection of infectious diseases such as tuberculosis[39] and Zika.[40] Our device is simple, low cost, and amenable to mass production and thus highly applicable to POC.

Several improvements can be applied to our ddELISA approach. One improvement is to reduce the time to image the droplet arrays. Since most droplets do not contain a bead, it is not necessary to image all droplets. Sorting the droplets to retain only the relevant droplets can be accomplished by dielectrophoretic,[41] magnetic,[42] acoustic,[43] or optical[44] approaches. Integrating droplet sorting can result in some bead loss and thus reduce the number of beads that are analyzed. However, based on our theoretical calculations, we show that as long as ∼50% of the beads are analyzed, maximal sensitivity can still be achieved. Additionally, approaches to image droplet arrays using wide-field fluorescent imaging have been previously developed and can be used to substantially reduce imaging times.[45] The second improvement is to reduce the

https://dx.doi.org/10.1021/acsnano.0c02378
ACS Nano XXXX, XXX, XXX−XXX

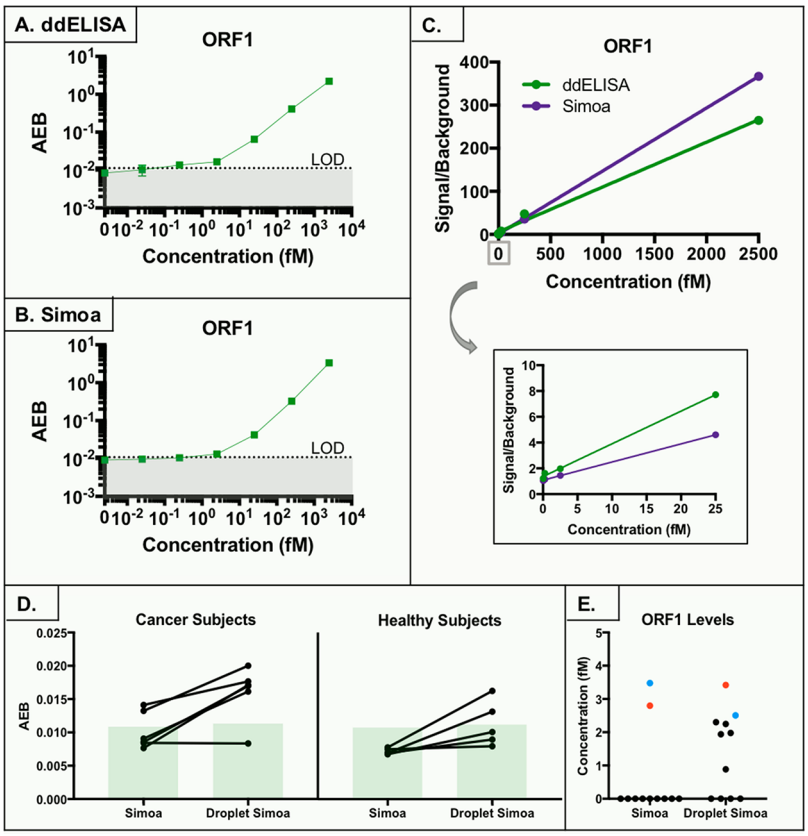

Figure 6. ORF1 assay and serum levels. (A) Calibration curve for ddELISA. B. Calibration curve for the conventional Simoa. (C) Signal over background of the ddELISA and conventional Simoa calibration curves. Zoomed in view from 0.025 to 25 fM (bottom). (D) Measured AEB values of ORF1 using Simoa and ddELISA in cancer and healthy serum. (E) Measured concentration values of ORF1 using Simoa and ddELISA. Samples from the same subject are colored. Samples below the detection limit were set to 0 fM.

time required for the fluorescent signal to become detectable. Due to the larger volume of the ddELISA droplets (picoliter) compared to the Simoa microwells (femtoliter), the time it takes for the fluorescent product of the enzyme−substrate reaction to be detectable is increased. Thus, other enzyme-based[46,47] or enzyme-free[48] approaches for signal amplification can be used to reduce the time to generate a detectable signal.

Improving the LODs to attomolar levels, and possibly even lower, allows for detection of proteins that have not previously been measured in biological samples such as blood, urine, and saliva. Additionally, some proteins cannot be measured in all subjects due to limitations in sensitivity, and therefore, their utility as biomarkers is limited. Since many protein biomarkers are present at low concentrations or are only measurable when the disease has progressed, improved sensitivity can facilitate biomarker discovery for various diseases including neurological diseases, infectious diseases, and cancer. New protein biomarkers can be used to diagnose disease early, to monitor response to treatment, or as companion diagnostics. Additionally, other biomarkers, such as microRNAs,[49] which are present at low levels in many biological samples, can also be measured with improved sensitivity over previously developed Simoa assays. Thus, ddELISA is highly promising for improved ultrasensitive detection of analytes.

METHODS

Microfluidic Device Fabrication. All microfluidic devices used in this paper were fabricated using polydimethylsiloxane (PDMS) with the standard soft lithographic methods.[24] Briefly, a thin layer of SU8-3010 (MicroChem) was spin coated onto the surface of a silicon wafer. After baking, a photomask was placed on top of the wafer for UV exposure. Propylene glycol methyl ether acetate (PGMEA) (Sigma-Aldrich, 537543) was then used to remove the unexposed SU8 from the wafer. After baking, the wafer was placed in a Petri dish and served as a mold for downstream PDMS fabrication. PDMS was well mixed with curing agent at a 10:1 ratio, degassed, poured onto the wafer, and placed in a 65 °C oven for at least 1.5 h. The PDMS was then cut and carefully peeled off from the mold. Holes for the inlets and outlets were formed using a 1 mm biopsy punch (Harris Uni-Core, Ted Pella, Inc.). The device and a clean glass slide were bonded to each other after plasma treatment. The devices were then treated with a hydrophobic surface treatment by flowing through Aquapel (PPG) followed by pressured nitrogen blow.

Droplet Generation. After immunocomplex formation (described in more detail in section 1.6), the beads were resuspended in a 2 μL solution containing 1.7 μL of substrate and 0.3 μL (15% v/v) of a density gradient solution Optiprep (Sigma, D1556) in a PCR tube. The solution was then mixed over 30 times using a pipet to resuspend the beads. A 1 mL syringe (BD Luer-Lok 1 mL Syringe, Beckton Dickinson) with 300 μL of HFE 7500 oil (3M) was connected with a needle (Vita Needles D929_SS27X0.5, 27 gauge, 0.5″) and PE/2 tubing (inner diameter: 0.38 mm, Scientific Commodities, Inc.) The HFE 7500 oil was pushed manually until the oil was approximately 0.5 cm away from the tip of the tubing. The tip of the tubing was then inserted into the PCR tube containing the bead solution, which was withdrawn into the tubing by slowly pulling the syringe's plunger. Then, 1 μL of HFE 7500 oil was added in a similar manner. The syringe was then loaded onto a syringe pump (Harvard Apparatus) and the tubing was inserted into the bead inlet on the droplet generating device. A second syringe was prepared by adding a solution containing HFE 7500 oil with 2% Fluorosurfactant

https://dx.doi.org/10.1021/acsnano.0c02378
ACS Nano XXXX, XXX, XXX−XXX

(008-FluoroSurfactant, Ran Biotechnologies). This second syringe was then connected with a needle and tubing and loaded onto a second syringe pump. The tubing was then inserted into the oil inlet on the droplet generating device. A pipet tip (VWR 37001-150) was inserted into the outlet for droplet collection. After this setup was complete, the syringe pumps were turned on. The flow rate of the bead solution was 80 μL/h, and the flow rate of the oil and surfactant solution was 120 μL/h. Monodispersed droplets with a diameter of ~14 μm (1.4 pL) were generated at a rate of ~20,000 Hz in under 1 min for a total of ~1.4 × 10^6 droplets. The droplets were then transferred from the pipet tip to a PCR tube and stored at 4 °C overnight and then imaged the next day.

Droplet Reinjection for Imaging. Prior to loading the droplets into the imaging chamber, the chamber was flushed with a solution of HFE 7500 oil and 2% surfactant. A 1 mL syringe containing 300 μL of HFE 7500 with 2% surfactant was then prepared for loading the droplets into the chamber. The oil solution was pushed manually until it was approximately 0.5 cm away from the tip of the tubing. The tip of the tubing was then inserted into the PCR tube containing the droplets and the droplet solution was withdrawn into the tubing by slowly pulling the syringe's plunger until all of the droplets were inside the tubing. The syringe was then loaded onto the syringe pump. The tip of the tubing was then pointed down for ~3 min. Due to gravity and the density difference between the droplets and the oil, the droplets will flow to the top of the tubing and a clear separation between the droplets and the oil solution can be observed. This technique allows us to closely pack the droplets, which is desirable for droplet loading. The tubing was then inserted into the inlet of the imaging chamber device and the pump was set to a flow rate of 100 μL/hour until all the droplets have been loaded into the imaging chamber (~5 min). The tubing was then removed from the inlet and the chamber was then imaged.

Imaging of Droplets inside the Chamber. The imaging chamber device was mounted on a motorized stage (Prior) on an IX83 microscope (Olympus). The imaging chamber was imaged in three different channels. First, a fluorescence image to identify "on droplets" by detecting the presence of the fluorescent product of the enzyme was obtained using a GFP filter (1 s exposure). Second, a fluorescence image to detect the dye-labeled beads was obtained using a Cy5 filter (1 s exposure). Third, a brightfield image (1 ms exposure) was obtained to identify the droplets. The images were obtained using a 10× objective and were acquired with a CCD Flash4 camera (Hamamatsu). The stage and the camera were controlled by commercial software (cellSens). Each frame was imaged in the three channels and then the stage moved automatically to the next frame. Total imaging time per chamber was approximately 15−20 min.

Image Analysis. First, the droplets were identified using the brightfield image. The droplet regions were isolated using Laplacian of Gaussian edge detection followed by morphological region filling. A watershed algorithm was applied to large regions to separate any partially connected regions. Then, the beads were located using the bead fluorescent image. Each bead was assigned to a droplet based on maximal overlap with a given droplet using a nearest neighbor algorithm. Then, the median intensity of each droplet was determined using the fluorescent image of the enzyme's product. A local background correction was then applied to account for lack of overall uniformity in the fluorescent image. Each droplet was matched with its five nearest droplet neighbors that did not contain a bead. If a droplet had too few neighbors within 1.5 times its diameter, the droplet was excluded from analysis. Once the droplet was matched with its five neighbors, the median intensity value of these five neighboring droplets was obtained and then subtracted from the intensity value of the droplet. Using this approach, a local background correction was applied.

After each droplet was assigned a corrected intensity value, we had to determine the intensity cutoff for the "on droplets." To do this, we used the intensities of the droplets that do not contain a bead since these droplets do not have enzymatic activity and can be considered true "off droplets." The intensity distribution of these "off droplets" closely follows a Gaussian distribution. Thus, a Guassian fit was applied and the mean and standard deviation were determined. To determine which droplets were "on", a cutoff was set at 10 standard deviations above the mean, and any bead-containing droplet with an intensity value above this cutoff was counted as "on". The fraction on was then calculated as the total number of "on" droplets over the total number of beads and then converted to AEB. All image processing and fitting was done using Matlab. Additional information on this process is provided in the Supporting Information.

Preparation of Antibody Coated Capture Beads and Biotinylated Detector Antibodies. Capture antibodies for IFNγ (BioLegend 507502) and IL-2 (Fisher/R&D Systems MAB602) were reconstituted and stored according to the instructions provided by the manufacturer. Each antibody was buffer exchanged to remove the storage buffer by first adding 0.13 mg of antibody solution to an Amicon filter (50K, Millipore). Bead Conjugation Buffer (Quanterix) was then added to the filter up to a total volume of 500 μL. The filter device was centrifuged at 14,000g for 5 min. The effluent was discarded and the process was repeated twice. The filter was inverted into a new tube and centrifuged at 1000g for 2 min. The filter was rinsed with 50 μL of Bead Conjugation Buffer and centrifuged at 1000g for 2 min. The concentration of the antibody was measured using a NanoDrop spectrophotometer. The IFNγ, and IL-2 capture antibodies were then diluted to 0.5 mg/mL and the ORF1 capture antibody (provided by Professor John LaCava) was diluted to 0.025 mg/mL in Bead Conjugation Buffer and stored on ice until ready for use. 2.8 × 10^8 dye-encoded carboxylated, 2.7 μm, paramagnetic beads (Quanterix) were transferred into a microtube and washed three times with 200 μL of Bead Wash Buffer (Quanterix). The beads were then washed two times with 200 μL of Bead Conjugation Buffer and resuspended in 190 μL of Bead Conjugation Buffer. Fresh 10 mg of 1-ethyl-3-(3-(dimethylamino)propyl) carbodiimide hydrochloride (EDC) (ThermoFisher) was reconstituted in 1 mL of Bead Conjugation Buffer just prior to use. To activate the beads, 10 μL of EDC was added to the bead suspension to give a final concentration of 0.5 mg/mL and a final volume of 200 μL. The beads were then placed on a rotator for 30 min. The activated beads were then washed with 200 μL of Bead Conjugation Buffer. 200 μL of capture antibody solution was then added to the beads, vortexed, and placed on the rotator for 120 min for conjugation. The antibody-conjugated beads were then washed two times with 200 μL of Bead Wash Buffer. The beads were then blocked with 200 μL of Bead Blocking Buffer (Quanterix) and placed on the rotator for 30 min. The beads were washed with 200 μL of Bead Wash Buffer, washed with 200 μL of Bead Diluent (Quanterix), and resuspended in 200 μL of Bead Diluent. The beads were counted using a Beckman Coulter multisizer and stored at 4 °C.

Detector antibodies were biotinylated as previously described.[50] Briefly, NHS-LC-LC-Biotin (ThermoFisher A35358) was used to biotinylate the detection antibodies. Here, 160× molar fold excess biotin was used for biotinylation of the IFNγ detection antibody (Fisher/R&D Systems MAB285), 320× molar fold excess biotin was used for biotinylation of the IL-2 detection antibody (Fisher/R&D Systems MAB202), and 80× molar fold excess was used for biotinylation of the ORF1 detection antibody (Abcam ab246317). The same reagent preparations were used for both the ddELISA assay format developed here and the conventional Simoa using the HD-1 Analyzer.

Preparation of Reagents and Immunoassay Assay Setup. Antibody-coated capture beads were diluted in Sample Diluent (Quanterix). A total of 100,000 beads per sample were used for the ddELISA assay, and 500,000 beads per sample were used for the conventional Simoa assay. Biotinylated detector antibodies were diluted in Detector Diluent (Quanterix) to the desired concentration. Streptavidin-β-galactosidase (SβG) Concentrate (Quanterix) was diluted to in SβG Diluent (Quanterix) to the desired concentration. Recombinant protein standards (Fisher/R&D Systems 285-IF and Systems 202-IL) were serially diluted to desired concentrations in Sample Diluent. Either three- or two-step assay configurations were chosen. Additional information on assay configuration and incubation

https://dx.doi.org/10.1021/acsnano.0c02378
ACS Nano XXXX, XXX, XXX−XXX

times for each assay is provided in Table 2. Incubation times were the same for each marker for both the ddELISA assay and the conventional Simoa assay using the HD-1 Analyzer.

Table 2

assay configuration				
target	assay setup	incubation times (min)	detector antibody concn	SβG concn
IFNγ	two-step	120−10	0.2 μg/mL	50 pM
IL-2	three-step	120−10−10	0.3 μg/mL	50 pM
ORF1	three-step	15−10−10	0.1 μg/mL	150 pM

In a three-step assay configuration, 25 μL of bead solution and 100 μL of sample were pipetted into a reaction cuvette and allowed to incubate. The beads were then pelleted with a magnet and the supernatant was removed. Following several washes, 100 μL of detector antibody was added and incubated. The beads were then pelleted with a magnet, and the supernatant was removed. Following a series of washes, 100 μL of SβG was added and incubated. The beads were washed, resuspended in substrate solution, and loaded onto the array or into droplets for single molecule analysis. In a two-step assay configuration, 25 μL of bead solution, 100 μL of sample, and 20 μL of detector antibody were pipetted into a reaction cuvette and allowed to incubate. The beads were then pelleted with a magnet, the supernatant was removed. Following several washes, 100 μL of SβG was added and incubated. The beads were washed, resuspended in substrate solution, and loaded onto the array or into droplets for single molecule analysis.

For the Simoa assay, the reagents including beads, detector, and SβG were placed in plastic bottles (Quanterix). The samples, including calibrators and serum samples, were loaded into a 96-well plate (Quanterix). All reagents (capture beads, detector antibodies, SβG, enzyme substrate resorufin β-D-galactopyranoside (RGP), Wash Buffer 1, Wash Buffer 2, and Simoa Sealing Oil were purchased from Quanterix and loaded into the Simoa HD-1 Analyzer (Quanterix) based on the manufacturer's instructions. All incubation and washes were conducted automatically using the HD-1 Analyzer. Following loading of the beads, the array was then sealed with oil and imaged. Images of the arrays were analyzed and AEB (average enzyme per bead) values were calculated by the software in the HD-1 Analyzer. Detailed information on the Simoa HD-1 Analyzer has been previously reported.[16]

For the ddELISA assay, the samples and reagents were loaded into a 96-well plate (Corning, CLS3651) and incubated as described. All washes were conducted automatically using Wash Buffer 1 and a microplate washer (BioTek). After the last wash, the beads were resuspended in 2 μL of the substrate solution, which consists of 1.7 μL of 100 μM FDG (fluorescein di-β-D-galactopyranoside) (Sigma) and 0.3 μL of Optiprep (Sigma). The bead solution was thoroughly mixed using a pipet and then loaded into the microfluidic device for partitioning into droplets.

Preparation of Serum Samples and Data Analysis. Serum samples from healthy and breast cancer subjects were purchased from BioIVT. Serum samples along with calibration curves were measured using both ddELISA developed here and the Simoa HD-1 Analyzer. Serum samples were diluted 4-fold in sample diluent (Quanterix). Plotted concentrations reflect measured values. The calibration curves were fit using a 4PL fit. The calibration curves were used to determine concentrations of the unknown serum samples. This analysis was done using the GraphPad Prism. All measurements were performed in 3−5 replicates. The limit of detection (LOD) of each assay was calculated as three standard deviations (SDs) above the background. The signal over background was calculated by taking the average signal of replicate measurements at a given concentration and dividing by the average background of replicate measurements. R^2 values for each calibration curve are shown in Supplementary Table 1.

ASSOCIATED CONTENT

Supporting Information

The Supporting Information is available free of charge at https://pubs.acs.org/doi/10.1021/acsnano.0c02378.

Additional details on the data and image analyses conducted in this study as well as supporting experimental data; additional details on processing the droplet images, including the brightfield and bead images, and integrating the three image layers (i.e., droplets, beads, and fluorescent intensity of the enzyme's substrate); additional information on image background correction; calibration curve characteristics, including histograms for the IFNγ and IL-2 ddELISAs, LODs based on the percentage of beads analyzed, and R^2 values of the Simoa and ddELISA calibration curves; additional information on the theoretical calculations (PDF)

AUTHOR INFORMATION

Corresponding Author

David R. Walt − *Wyss Institute for Biologically Inspired Engineering and Department of Chemical Biology, Harvard University, Boston, Massachusetts 02115, United States; Department of Pathology, Brigham and Women's Hospital, Harvard Medical School, Boston, Massachusetts 02115, United States;* orcid.org/0000-0002-5524-7348; Email: dwalt@bwh.harvard.edu

Authors

Limor Cohen − *Wyss Institute for Biologically Inspired Engineering and Department of Chemical Biology, Harvard University, Boston, Massachusetts 02115, United States; Department of Pathology, Brigham and Women's Hospital, Harvard Medical School, Boston, Massachusetts 02115, United States;* orcid.org/0000-0003-1448-0925

Naiwen Cui − *School of Engineering and Applied Sciences, Harvard University, Cambridge, Massachusetts 02138, United States*

Yamei Cai − *School of Engineering and Applied Sciences, Harvard University, Cambridge, Massachusetts 02138, United States*

Padric M. Garden − *Wyss Institute for Biologically Inspired Engineering, Harvard University, Boston, Massachusetts 02115, United States; Department of Pathology, Brigham and Women's Hospital, Harvard Medical School, Boston, Massachusetts 02115, United States;* orcid.org/0000-0002-2161-2730

Xiang Li − *Wyss Institute for Biologically Inspired Engineering, Harvard University, Boston, Massachusetts 02115, United States; Department of Pathology, Brigham and Women's Hospital, Harvard Medical School, Boston, Massachusetts 02115, United States;* orcid.org/0000-0001-8029-8983

David A. Weitz − *Wyss Institute for Biologically Inspired Engineering and School of Engineering and Applied Sciences, Harvard University, Boston, Massachusetts 02115, United States;* orcid.org/0000-0001-6678-5208

Complete contact information is available at: https://pubs.acs.org/10.1021/acsnano.0c02378

Author Contributions

[⊥]L.C. and N.C. are co-first authors. D.R.W. and L.C. designed the study. N.C. and Y.C. designed and fabricated the microfluidic devices under the guidance of D.A.W. L.C., P.M.G, N.C., and Y.C. performed the experiments. P.M.G.

https://dx.doi.org/10.1021/acsnano.0c02378
ACS Nano XXXX, XXX, XXX−XXX

developed the algorithms for the image analysis. L.C., P.M.G, N.C., and Y.C. analyzed the data. X.L. performed the theoretical calculations. L.C. and D.R.W wrote the manuscript with input from all other authors.

Notes

The authors declare the following competing financial interest(s): D.R.W. has a financial interest in Quanterix Corporation, a company that develops an ultrasensitive digital immunoassay platform. He is an inventor of the Simoa technology, a founder of the company and also serves on its Board of Directors. Interests of D.R.W. were reviewed and are managed by BWH and Partners HealthCare in accordance with their conflict of interest policies. All other authors declare no competing financial interest.

ACKNOWLEDGMENTS

The authors would like to thank J. LaCava of Rockefeller University for providing us with a nanobody for ORF1 and ORF1 recombinant protein. The authors would also like to thank M. Taylor and K. Burns for helpful discussions on ORF1 as a biomarker. This work was supported by the National Science Foundation (DMR-1708729) and the NSF-funded Harvard Materials Research Science and Engineering Center (DMR-1420570). N.C. would also like to thank NSERC for providing the PGS-D scholarship.

REFERENCES

(1) Anderson, N. L.; Anderson, N. G. The Human Plasma Proteome: History, Character, and Diagnostic Prospects. *Mol. Cell. Proteomics* **2002**, *1*, 845−867.

(2) Anderson, N. L. The Clinical Plasma Proteome: A Survey of Clinical Assays for Proteins in Plasma and Serum. *Clin. Chem.* **2010**, *56*, 177−185.

(3) Uhlén, M.; Karlsson, M. J.; Hober, A.; Svensson, A.-S.; Scheffel, J.; Kotol, D.; Zhong, W.; Tebani, A.; Strandberg, L.; Edfors, F.; Sjöstedt, E.; Mulder, J.; Mardinoglu, A.; Berling, A.; Ekblad, S.; Dannemeyer, M.; Kanje, S.; Rockberg, J.; Lundqvist, M.; Malm, M.; et al. The Human Secretome. *Sci. Signaling* **2019**, *12*, No. eaaz0274.

(4) Cohen, L.; Walt, D. R. Highly Sensitive and Multiplexed Protein Measurements. *Chem. Rev.* **2019**, *119*, 293.

(5) Gorris, H. H.; Rissin, D. M.; Walt, D. R. Stochastic Inhibitor Release and Binding from Single-Enzyme Molecules. *Proc. Natl. Acad. Sci. U. S. A.* **2007**, *104*, 17680−17685.

(6) Rissin, D. M.; Gorris, H. H.; Walt, D. R. Distinct and Long-Lived Activity States of Single Enzyme Molecules. *J. Am. Chem. Soc.* **2008**, *130*, 5349−5353.

(7) Rissin, D. M.; Walt, D. R. Digital Readout of Target Binding with Attomole Detection Limits *via* Enzyme Amplification in Femtoliter Arrays. *J. Am. Chem. Soc.* **2006**, *128*, 6286−6287.

(8) Rissin, D. M.; Walt, D. R. Digital Concentration Readout of Single Enzyme Molecules Using Femtoliter Arrays and Poisson Statistics. *Nano Lett.* **2006**, *6*, 520−523.

(9) Rissin, D. M.; Kan, C. W.; Campbell, T. G.; Howes, S. C.; Fournier, D. R.; Song, L.; Piech, T.; Patel, P. P.; Chang, L.; Rivnak, A. J.; Ferrell, E. P.; Randall, J. D.; Provuncher, G. K.; Walt, D. R.; Duffy, D. C. Single-Molecule Enzyme-Linked Immunosorbent Assay Detects Serum Proteins at Subfemtomolar Concentrations. *Nat. Biotechnol.* **2010**, *28*, 595−599.

(10) Cohen, L.; Walt, D. R. Single-Molecule Arrays for Protein and Nucleic Acid Analysis. *Annu. Rev. Anal. Chem.* **2017**, *10*, 345−363.

(11) Wu, C.; Maley, A. M.; Walt, D. R. Single-Molecule Measurements in Microwells for Clinical Applications. *Crit. Rev. Clin. Lab. Sci.* **2020**, *57*, 270−290.

(12) Baird, A. L.; Westwood, S.; Lovestone, S. Blood-Based Proteomic Biomarkers of Alzheimer's Disease Pathology. *Front. Neurol.* **2015**, *6*, 236.

(13) Hanash, S. M.; Pitteri, S. J.; Faca, V. M. Mining the Plasma Proteome for Cancer Biomarkers. *Nature* **2008**, *452*, 571−579.

(14) Gilboa, T.; Garden, P. M.; Cohen, L. Single-Molecule Analysis of Nucleic Acid Biomarkers - a Review. *Anal. Chim. Acta* **2020**, *1115*, 61.

(15) Wu, D.; Milutinovic, M. D.; Walt, D. R. Single Molecule Array (Simoa) Assay with Optimal Antibody Pairs for Cytokine Detection in Human Serum Samples. *Analyst* **2015**, *140*, 6277−6282.

(16) Wilson, D. H.; Rissin, D. M.; Kan, C. W.; Fournier, D. R.; Piech, T.; Campbell, T. G.; Meyer, R. E.; Fishburn, M. W.; Cabrera, C.; Patel, P. P.; Frew, E.; Chen, Y.; Chang, L.; Ferrell, E. P.; von Einem, V.; McGuigan, W.; Reinhardt, M.; Sayer, H.; Vielsack, C.; Duffy, D. C. The Simoa HD-1 Analyzer: A Novel Fully Automated Digital Immunoassay Analyzer with Single-Molecule Sensitivity and Multiplexing. *J. Lab. Autom.* **2016**, *21*, 533−547.

(17) Barbee, K. D.; Hsiao, A. P.; Heller, M. J.; Huang, X. Electric Field Directed Assembly of High-Density Microbead Arrays. *Lab Chip* **2009**, *9*, 3268−3274.

(18) Shang, L.; Cheng, Y.; Zhao, Y. Emerging Droplet Microfluidics. *Chem. Rev.* **2017**, *117*, 7964−8040.

(19) Hindson, B. J.; Ness, K. D.; Masquelier, D. A.; Belgrader, P.; Heredia, N. J.; Makarewicz, A. J.; Bright, I. J.; Lucero, M. Y.; Hiddessen, A. L.; Legler, T. C.; Kitano, T. K.; Hodel, M. R.; Petersen, J. F.; Wyatt, P. W.; Steenblock, E. R.; Shah, P. H.; Bousse, L. J.; Troup, C. B.; Mellen, J. C.; Wittmann, D. K.; et al. High-Throughput Droplet Digital PCR System for Absolute Quantitation of DNA Copy Number. *Anal. Chem.* **2011**, *83*, 8604−8610.

(20) Hindson, C. M.; Chevillet, J. R.; Briggs, H. A.; Gallichotte, E. N.; Ruf, I. K.; Hindson, B. J.; Vessella, R. L.; Tewari, M. Absolute Quantification by Droplet Digital PCR *versus* Analog Real-Time PCR. *Nat. Methods* **2013**, *10*, 1003−1005.

(21) Klein, A. M.; Mazutis, L.; Akartuna, I.; Tallapragada, N.; Veres, A.; Li, V.; Peshkin, L.; Weitz, D. A.; Kirschner, M. W. Droplet Barcoding for Single-Cell Transcriptomics Applied to Embryonic Stem Cells. *Cell* **2015**, *161*, 1187−1201.

(22) Macosko, E. Z.; Basu, A.; Satija, R.; Nemesh, J.; Shekhar, K.; Goldman, M.; Tirosh, I.; Bialas, A. R.; Kamitaki, N.; Martersteck, E. M.; Trombetta, J. J.; Weitz, D. A.; Sanes, J. R.; Shalek, A. K.; Regev, A.; McCarroll, S. A. Highly Parallel Genome-Wide Expression Profiling of Individual Cells Using Nanoliter Droplets. *Cell* **2015**, *161*, 1202−1214.

(23) Prakadan, S. M.; Shalek, A. K.; Weitz, D. A. Scaling by Shrinking: Empowering Single-Cell "Omics" with Microfluidic Devices. *Nat. Rev. Genet.* **2017**, *18*, 345−361.

(24) Mazutis, L.; Gilbert, J.; Ung, W. L.; Weitz, D. A.; Griffiths, A. D.; Heyman, J. A. Single-Cell Analysis and Sorting Using Droplet-Based Microfluidics. *Nat. Protoc.* **2013**, *8*, 870−891.

(25) Abbaspourrad, A.; Zhang, H.; Tao, Y.; Cui, N.; Asahara, H.; Zhou, Y.; Yue, D.; Koehler, S. A.; Ung, L. W.; Heyman, J.; Ren, Y.; Ziblat, R.; Chong, S.; Weitz, D. A. Label-Free Single-Cell Protein Quantification Using a Drop-Based Mix-And-Read System. *Sci. Rep.* **2015**, *5*, 12756.

(26) Cui, N.; Zhang, H.; Schneider, N.; Tao, Y.; Asahara, H.; Sun, Z.; Cai, Y.; Koehler, S. A.; de Greef, T. F. A.; Abbaspourrad, A.; Weitz, D. A.; Chong, S. A Mix-and-Read Drop-Based *In Vitro* Two-Hybrid Method for Screening High-Affinity Peptide Binders. *Sci. Rep.* **2016**, *6*, 22575.

(27) Shahi, P.; Kim, S. C.; Haliburton, J. R.; Gartner, Z. J.; Abate, A. R. Abseq: Ultrahigh-Throughput Single Cell Protein Profiling with Droplet Microfluidic Barcoding. *Sci. Rep.* **2017**, *7*, 44447.

(28) Shim, J. U.; Ranasinghe, R. T.; Smith, C. A.; Ibrahim, S. M.; Hollfelder, F.; Huck, W. T. S.; Klenerman, D.; Abell, C. Ultrarapid Generation of Femtoliter Microfluidic Droplets for Single-Molecule-Counting Immunoassays. *ACS Nano* **2013**, *7*, 5955−5964.

(29) Yelleswarapu, V.; Buser, J. R.; Haber, M.; Baron, J.; Inapuri, E.; Issadore, D. Mobile Platform for Rapid Sub-Picogram-Per-Milliliter, Multiplexed, Digital Droplet Detection of Proteins. *Proc. Natl. Acad. Sci. U. S. A.* **2019**, *116*, 4489−4495.

https://dx.doi.org/10.1021/acsnano.0c02378
ACS Nano XXXX, XXX, XXX−XXX

(30) Rissin, D. M.; Fournier, D. R.; Piech, T.; Kan, C. W.; Campbell, T. G.; Song, L.; Chang, L.; Rivnak, A. J.; Patel, P. P.; Provuncher, G. K.; Ferrell, E. P.; Howes, S. C.; Pink, B. A.; Minnehan, K. A.; Wilson, D. H.; Duffy, D. C. Simultaneous Detection of Single Molecules and Singulated Ensembles of Molecules Enables Immunoassays with Broad Dynamic Range. *Anal. Chem.* **2011**, *83*, 2279−2285.
(31) Kan, C. W.; Rivnak, A. J.; Campbell, T. G.; Piech, T.; Rissin, D. M.; Mösl, M.; Peterça, A.; Niederberger, H.-P.; Minnehan, K. a.; Patel, P. P.; Ferrell, E. P.; Meyer, R. E.; Chang, L.; Wilson, D. H.; Fournier, D. R.; Duffy, D. C. Isolation and Detection of Single Molecules on Paramagnetic Beads Using Sequential Fluid Flows in Microfabricated Polymer Array Assemblies. *Lab Chip* **2012**, *12*, 977.
(32) Sakakihara, S.; Araki, S.; Iino, R.; Noji, H. A Single-Molecule Enzymatic Assay in a Directly Accessible Femtoliter Droplet Array. *Lab Chip* **2010**, *10*, 3355−3362.
(33) Xiao-Jie, L.; Hui-Ying, X.; Qi, X.; Jiang, X.; Shi-Jie, M. LINE-1 in Cancer: Multifaceted Functions and Potential Clinical Implications. *Genet. Med.* **2016**, *18*, 431−439.
(34) Ardeljan, D.; Taylor, M. S.; Ting, D. T.; Burns, K. H. The Human Long Interspersed Element-1 Retrotransposon: An Emerging Biomarker of Neoplasia. *Clin. Chem.* **2017**, *63*, 816−822.
(35) Burns, K. H. Transposable Elements in Cancer. *Nat. Rev. Cancer* **2017**, *17*, 415−424.
(36) Kim, S. H.; Iwai, S.; Araki, S.; Sakakihara, S.; Iino, R.; Noji, H. Large-Scale Femtoliter Droplet Array for Digital Counting of Single Biomolecules. *Lab Chip* **2012**, *12*, 4986−4991.
(37) Ono, T.; Ichiki, T.; Noji, H. Digital Enzyme Assay Using Attoliter Droplet Array. *Analyst* **2018**, *143*, 4923−4929.
(38) Rusling, J. F.; Kumar, C. V.; Gutkind, J. S.; Patel, V. Measurement of Biomarker Proteins for Point-of-Care Early Detection and Monitoring of Cancer. *Analyst* **2010**, *135*, 2496−2511.
(39) Ahmad, R.; Xie, L.; Pyle, M.; Suarez, M. F.; Broger, T.; Steinberg, D.; Ame, S. M.; Lucero, M. G.; Szucs, M. J.; MacMullan, M.; Berven, F. S.; Dutta, A.; Sanvictores, D. M.; Tallo, V. L.; Bencher, R.; Eisinger, D. P.; Dhingra, U.; Deb, S.; Ali, S. M.; Mehta, S.; et al. A Rapid Triage Test for Active Pulmonary Tuberculosis in Adult Patients with Persistent Cough. *Sci. Transl. Med.* **2019**, *11*, No. eaaw8287.
(40) Rong, Z.; Wang, Q.; Sun, N.; Jia, X.; Wang, K.; Xiao, R.; Wang, S. Smartphone-Based Fluorescent Lateral Flow Immunoassay Platform for Highly Sensitive Point-of-Care Detection of Zika Virus Nonstructural Protein 1. *Anal. Chim. Acta* **2019**, *1055*, 140−147.
(41) Agresti, J. J.; Antipov, E.; Abate, A. R.; Ahn, K.; Rowat, A. C.; Baret, J.-C.; Marquez, M.; Klibanov, A. M.; Griffiths, A. D.; Weitz, D. A. Ultrahigh-Throughput Screening in Drop-Based Microfluidics for Directed Evolution. *Proc. Natl. Acad. Sci. U. S. A.* **2010**, *107*, 4004−4009.
(42) Zhang, K.; Liang, Q.; Ma, S.; Mu, X.; Hu, P.; Wang, Y.; Luo, G. On-Chip Manipulation of Continuous Picoliter-Volume Superparamagnetic Droplets Using a Magnetic Force. *Lab Chip* **2009**, *9*, 2992−2999.
(43) Franke, T.; Abate, A. R.; Weitz, D. A.; Wixforth, A. Surface Acoustic Wave (SAW) Directed Droplet Flow in Microfluidics for PDMS Devices. *Lab Chip* **2009**, *9*, 2625−2627.
(44) Jung, J. H.; Lee, K. H.; Lee, K. S.; Ha, B. H.; Oh, Y. S.; Sung, H. J. Optical Separation of Droplets on a Microfluidic Platform. *Microfluid. Nanofluid.* **2014**, *16*, 635−644.
(45) Hatch, A. C.; Fisher, J. S.; Tovar, A. R.; Hsieh, A. T.; Lin, R.; Pentoney, S. L.; Yang, D. L.; Lee, A. P. 1-Million Droplet Array with Wide-Field Fluorescence Imaging for Digital PCR. *Lab Chip* **2011**, *11*, 3838−3845.
(46) Konry, T.; Hayman, R. B.; Walt, D. R. Microsphere-Based Rolling Circle Amplification Microarray for the Detection of DNA and Proteins in a Single Assay. *Anal. Chem.* **2009**, *81*, 5777−5782.
(47) Gootenberg, J. S.; Abudayyeh, O. O.; Lee, J. W.; Essletzbichler, P.; Dy, A. J.; Joung, J.; Verdine, V.; Donghia, N.; Daringer, N. M.; Freije, C. A.; Myhrvold, C.; Bhattacharyya, R. P.; Livny, J.; Regev, A.; Koonin, E. V.; Hung, D. T.; Sabeti, P. C.; Collins, J. J.; Zhang, F. Nucleic Acid Detection with CRISPR-Cas13a/C2c2. *Science* **2017**, *356*, 438−442.
(48) Akama, K.; Shirai, K.; Suzuki, S. Droplet-Free Digital Enzyme-Linked Immunosorbent Assay Based on a Tyramide Signal Amplification System. *Anal. Chem.* **2016**, *88*, 7123−7129.
(49) Cohen, L.; Hartman, M. R.; Amardey-Wellington, A.; Walt, D. R. Digital Direct Detection of MicroRNAs Using Single Molecule Arrays. *Nucleic Acids Res.* **2017**, *45*, No. e137.
(50) Cohen, L.; Walt, D. R. Evaluation of Antibody Biotinylation Approaches for Enhanced Sensitivity of Single Molecule Array (Simoa) Immunoassays. *Bioconjugate Chem.* **2018**, *29*, 3452−3458.

https://dx.doi.org/10.1021/acsnano.0c02378
ACS Nano XXXX, XXX, XXX−XXX